

**Resolution of 3D bioprinting inside bulk gel and granular gel baths**

Journal:	<i>Soft Matter</i>
Manuscript ID	SM-REV-06-2021-000926.R1
Article Type:	Review Article
Date Submitted by the Author:	17-Aug-2021
Complete List of Authors:	Xie, Zheng-Tian; Osaka University, Graduate School of Engineering, Department of Applied Chemistry Kang, Dong-Hee; Osaka University, Graduate School of Engineering, Department of Applied Chemistry Matsusaki, Michiya; Osaka University, Graduate School of Engineering, Department of Applied Chemistry

ARTICLE

Resolution of 3D bioprinting inside bulk gel and granular gel baths

Zheng-Tian Xie, Dong-Hee Kang, and Michiya Matsusaki*

=Received 00th January 20xx,
Accepted 00th January 20xx

DOI: 10.1039/x0xx00000x

Three-dimensional (3D) bioprinting has rapidly developed in the last decade, playing an increasingly important role in applications including pharmacokinetics research, tissue engineering, and organ regeneration. As a cutting-edge technology in 3D printing, gel bath-supported 3D bioprinting enables the freeform construction of complex structures with soft and water-containing materials, facilitating the *in vitro* fabrication of live tissue or organ models. To realize *in vivo*-like organs or tissues in terms of biological function and complex structure by 3D printing, high resolution and fidelity are prerequisites. Although a wide range of gel matrices have recently been developed as supporting materials, the effect of the bath properties and printing parameters on the print resolution is still not clearly understood. This review systematically introduces the decisive factors for resolution in both bulk gel bath systems and granular microgel bath systems, providing guidelines for high-resolution 3D bioprinting based on the bath properties and printing parameters.

1. Introduction

Three-dimensional (3D) printing is a revolutionary technology that has emerged as a versatile and powerful platform for freeform construction of complex structures with programmable geometrical features and designable composition.¹⁻⁷ With the rapid growth of 3D printing in the last decade, a few pioneering studies have attempted to leverage this art for bio-applications such as *in vitro* fabrication of tissue models for pharmacokinetics research, drug screening,⁸⁻¹¹ and organ regeneration.¹²⁻¹⁴ It is clear that 3D bioprinting will play an increasingly important role in the fields of biomedical science, healthcare, and mechanical engineering in the near future.¹⁵

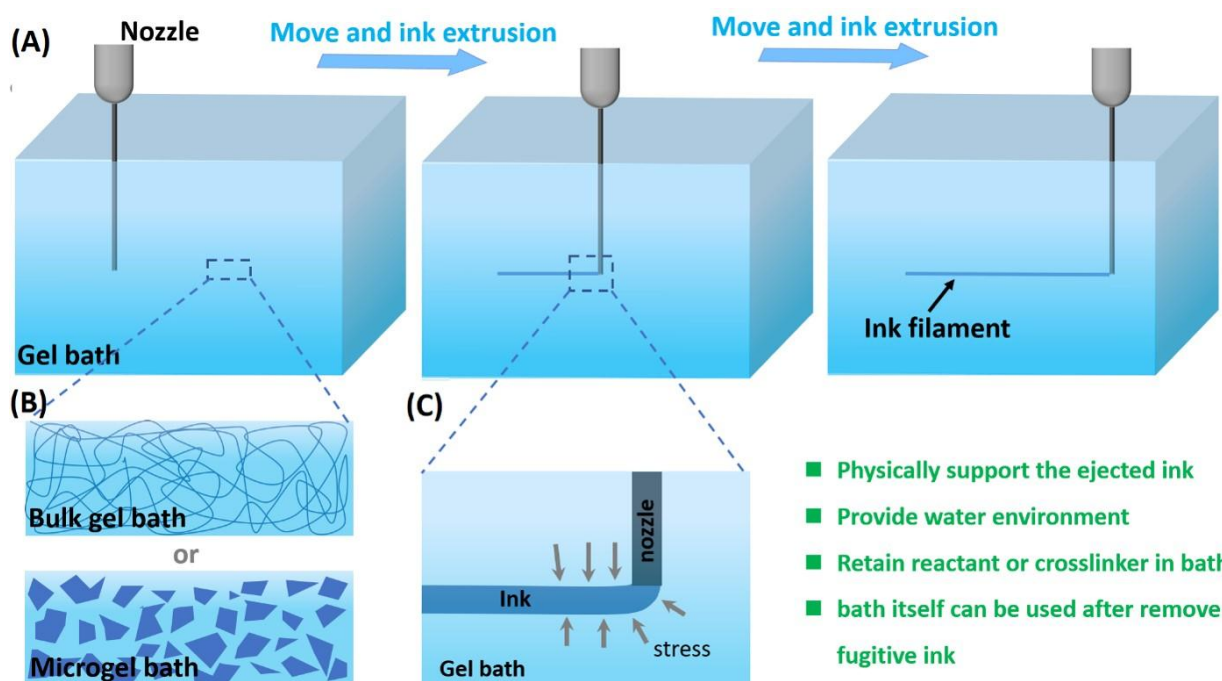
Based on the printing mechanism, 3D printing can be roughly classified into three categories including inkjet printing,^{16, 17} extrusion deposition¹⁸ and photo-curing printing.^{19, 20} Photo-curing printing such as digital light processing (DLP) and selective laser sintering (SLS) fundamentally exploits photo-cross-linkable materials,^{11, 21, 22} while most biocompatible materials are not available for rapid photo-crosslinking. Compared to inkjet printing that emits

micro-sized droplets, extrusion-based printing enables continuous dispensing. Moreover, this approach facilitates the printing of biomaterials with wide ranges of viscosity and composition including cells.^{5, 14, 23-25} For these reasons, extrusion-based 3D printing is preferred for *in vitro* tissue fabrication in most studies.²⁶ In the conventional extrusion-based printing, the liquified ink was layer-by-layer deposited onto a substrate using the programmed path to build up the designed structure.²⁷⁻²⁹ For the fabrication of a 3D structure, the newly ink after the move to the upper XY-plane is ejected and fused onto the preformed structure. After deposition, ink materials have to be mechanically strong enough to ensure shape fidelity and stability against gravitational force. The support structure also has to be printed together for holding the part of the 3D structure, and it will be removed after the completion of printing.³⁰ This method strictly limits the choice of ink materials and hinders the potential design and production of sophisticated 3D structures, presenting an obstacle to *in vitro* recapitulation of human organs or tissues that have geometrically complex architectures such as vascular networks, cartilage, and muscle.

Address: Department of Applied Chemistry, Graduate School of Engineering, Osaka University, 2-1 Yamadaoka, Suita, Osaka 565-0871, Japan

*Corresponding author. Email: m-matsus@chem.eng.osaka-u.ac.jp; Tel: +81-6-6879-7356; Fax: +81-6879-7359.

Electronic Supplementary Information (ESI) available: [details of any supplementary information available should be included here]. See DOI: 10.1039/x0xx00000x



Scheme 1 A. The printing process in a gel bath. B. Schemes of the morphology of a bulk gel bath and microgel bath, respectively. C. Magnified image of the nozzle region during the printing process. The ink is continuously ejected and then supported by the gel matrix.

To overcome this hurdle, bath-supported 3D printing (also called embedded printing) was developed from extrusion-based printing by introducing suitable bath materials such as gels, inorganic suspensions, and viscous polymer solutions to support and fix the ink filament.³⁰⁻³² Among them, hydrogels have been one of the most frequently used support materials in bioprinting due to their high water content, transparency, and self-healing properties.³³⁻³⁵ Thanks to the significant development of gel materials in recent years, various gels have been used as supporting materials in 3D bioprinting. As shown in **Scheme 1A** and **B**, in a typical bath-supported 3D printing system, a nozzle is embedded in the gel bath and translated in the bath matrix to realize the omnidirectional printing of ink along a programmed route through the movement of the nozzle. Meanwhile, the printed ink is immediately surrounded by the gel matrix after ejection, preventing ink flow or deformations caused by gravitational forces (**Scheme 1C**). In general, gel bath-supported 3D printing has several advantages: 1) it supports and fixes the printed filament and prevents the collapse or deformation of printed products, enabling printing of complex structures using soft biomaterials. 2) gel baths containing growth factors or ECM provide nutrients and a suitable water environment for cell-laden printing.^{36, 37} 3) some crosslinking agents can be retained in the gel bath for the post crosslinking of printed ink, endowing greater flexibility and more design possibilities for printing strategies.³⁸ 4) the gel bath itself can also be used for bio-applications such as vessel networks or models after removal of the fugitive ink, enabling the continuous printing of cell ink.³⁹ Gel bath-supported printing has opened up new opportunities and aroused great interest in the bioprinting field for tissue engineering and personalized therapy.⁴⁰ To

date, gel-supported bioprinting has been exploited to fabricate vessels,^{41, 42} and simple organ models⁴³⁻⁴⁷ in recent research.

Despite the recent advances in *in vitro* tissue or organ fabrication derived by gel-supported bioprinting, high resolution and fidelity are still sought after to manifest the structural hierarchies or complexity necessary for *in vivo*-like biological functions.^{7, 12, 48} In 2017, Hinton *et al.*⁴⁹ concluded that the size of the materials being deposited strongly affects the function of the fabricated structure as well as its application in tissue engineering. For example, blood capillaries in the human body play a crucial role in nutrient and oxygen transportation, while their diameter is on the scale of several micrometers.⁵⁰ *In vitro* printing of blood capillary, therefore, requires printing with resolutions in the micrometer scale. In 2019, Lee *et al.*⁵¹ presented an overview concerning the affecting factors and the assessing methods of the printing resolution in various bioprinting technologies including inkjet, extrusion, and photopolymerization. They denoted that the principles for improving the print resolution and accuracy differs in various bioprinting technology. A guideline for printability evaluation is to determine whether the fundamental units can be achieved specific to the bioprinting technology. In practical experiment, the resolution of 3D printing can be defined as the minimum size of the feature that can be attained. For bath-supported extrusion printing,⁴⁹ this basically depends on two factors: the minimum diameter of the filament that can be stably and continuously printed, and the positional accuracy of the filament in the bath after printing. The filament diameter is mainly related to printing parameters (e.g., nozzle size, ink ejection speed, nozzle moving speed, etc.) and bath rheology (yield stress, modulus, etc.). The positional accuracy is not only related to the rheological

properties of the bath and ink, but also involves the printing path and post-treatments. The different bath systems usually show distinct printing resolution, and the decisive factor determining the resolution in each bath condition also differs. Therefore, it is necessary to understand how the bath conditions and printing parameters dictate the final resolution and fidelity of the printed structure.

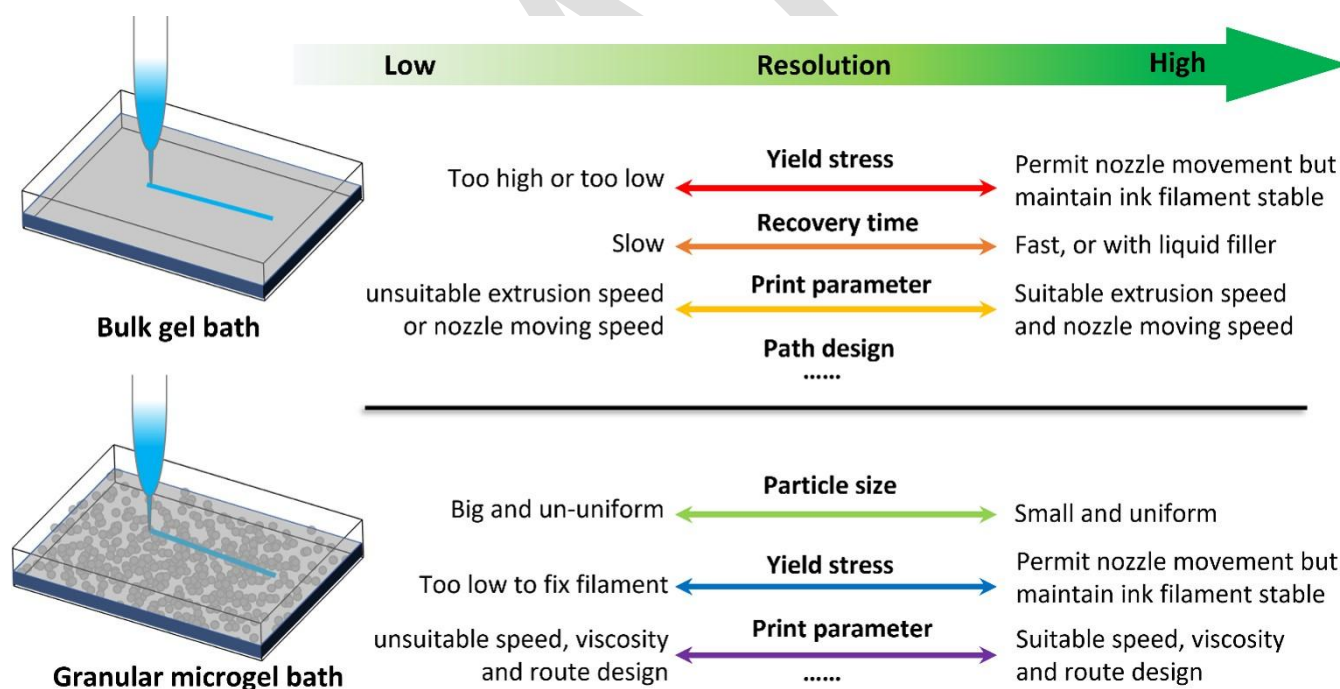
This review focuses on the resolution of gel bath-supported 3D printing, and attempts to elucidate the factors affecting the printing resolution in current bath systems. Based on comparative analysis of previous research, this review sets out to summarize the effects governing bath design and parameter selection for high-resolution bioprinting in a bath matrix. According to the morphology of bath systems, current gel-based bath systems can be roughly classified into two types: bulk gel baths and granular microgel baths. Considering that the resolution-decisive factors in different types of bath systems are also different, this review will introduce each of the bath systems separately, as shown in **Scheme 2**. Finally, while considering the current challenges of high-resolution 3D bioprinting, a brief discussion on the outlook for future research into bath-supported 3D printing is presented.

printing process, the printed ink was supported and fixed by the bath matrix. The rheological properties of the bath materials and the printing parameters are major effect factors for precise printing.

2.1 Effect of mechanical properties of bath on the resolution

2.1.1 Yield stress. Generally, a suitable polymer bulk gel bath for embedded 3D printing should be a thixotropic solution that not only possesses a shear-thinning characteristic with a relatively low yield stress, τ_y , allowing nozzle movement with less resistance, but also has sufficient storage modulus, G' , to stably support and anchor the ejected ink at a predetermined position.^{40, 54, 55}

During the printing process, the translation of the shaft of the needle in the bath may lead to a void or crevice around the nozzle and break the balance of the stress applied on the ejected ink, allowing the diffusion of ink into the crevices and eventually causing a deviation of the printed filament from the predetermined size and position. Therefore, for high-resolution printing in a bath system, the elimination of crevices or voids during nozzle movement is a basic precondition. To meet this requirement, current research is mainly based on two strategies for bath design. The first is to introduce a supplement solution to fill the crevices generated in the



Scheme 2 The factors affecting resolution of bath-supported 3D printing in a bulk gel bath and granular microgel bath.

2. Effect factors in bulk polymer gel baths

To realize spatial resolution for the patterning of a programmed structure with high fidelity, a suitable bath is essential. To the best of our knowledge, Lewis *et al.*⁴⁰ were the first to report on gel bath-based 3D printing exploiting the thixotropic behavior^{52, 53} of a bulk polymer gel. In a typical

printing process,^{40, 56} and the second is to rely on the recovery of the crevices through an effective deformation or self-healing behavior of the gel matrix. For the bath materials that show relatively high τ_y or lesser self-healing ability, the first strategy can be used. For example, Lewis *et al.*⁴⁰ developed a direct ink writing (DIW) method in 2011 for the fabrication of a microvascular network, in which an aqueous Pluronic F127 solution, a triblock copolymer, was used as a bath material to

support the printed structure. To prevent the crevices caused by the needle movement in the bulk gel, and ensure shape fidelity, they introduced a filler solution (a diacrylate-functionalized Pluronic F127 solution) in this bath system. As shown in **Fig. 1A** the filler solution was designed to be a liquid copolymer solution that covered the top surface of the bath, which has good flowability and can fill the crevice generated during the shaft movement. Since the filler solution was chemically identical to the bath material (both were diacrylate-functionalized Pluronic F127 but with varying concentrations), it can be crosslinked with the bath materials. Based on this strategy, filaments with sizes ranging from 18–600 μm were printed in their work.

However, the introduction of a filler material complicates the bath system and requires the delicate design of a filter with suitable flowability and good compatibility. In this context, many new gel matrices with self-recovery behavior have been exploited to support 3D bioprinting, which are usually thixotropic polymer solutions that show a shear-thinning characteristic when the nozzle is translating, but can quickly recover their stress after the removal of shear stress (**Fig. 1B**).⁵⁷ In other words, these bath matrices can keep a solid-like or highly viscous state at low shear rate, enabling them to support the printed structure, while exhibit a liquid-like state under high shear-rate, approving the free movement of nozzle within them. A bath with good recovery performance that can restructure at the microscale and mitigate crevice formation could remove the need for a filler solution without loss of print fidelity. Several reversible interactions such as guest-host interaction,^{58, 59} ion interaction, and metal coordination effect⁶⁰ can be used to design recoverable self-healing bath

matrices (**Fig. 1C and D**).

2.1.2 Recovery behavior. The recovery behavior of bath materials is closely associated with their mechanical properties, which can be tailored by adjusting the bath composition and the intermolecular interactions in the bath.^{14, 58} In 2015, Burdick *et al.*⁵⁸ printed linear supramolecular filaments in a self-healing hydrogel based on a guest-host interaction. The bath was prepared by modifying hyaluronic acid with either adamantane (Ad) or β -cyclodextrin (β -CD) (Ad-HA and CD-HA) and mixing them to form a supramolecular gel with self-healing properties. With the optimized composition ratio (Ad-HA and CD-HA with 40% of the HA repeat units modified, mixed at Ad: CD of 1:1 and at a total concentration of 4 wt/v%), the bath exhibited the requisite dynamic bond between CD and Ad. This endowed it with the requisite shear-thinning and self-healing properties for the 3D printing of a vascular network in it with a resolution of 35 μm .⁵⁸ They⁵⁹ also improved the bath system by encompassing thiol-ene crosslinking that permits the stabilization of the support hydrogel while incorporating both cell adhesion and cell-mediated degradation, as well as a polydimethylsiloxane (PDMS) device that can be used for the printing and culturing of vascularized constructs. Xanthan gum (XG)³⁹ has also been reported as a thixotropic polymer to support the 3D printing of an alginate filament in the bath. The viscosity of the XG supporting matrix showed an exponential decrease as the shear rate was increased. Moreover, it can be easily removed to release the product by simply immersing the sample in water, preserving its structural integrity. This bath enabled the printing of a perfusable tube and the finest filament diameter reported in this work was about 350 μm . In 2019, Bruna *et al.*³⁸

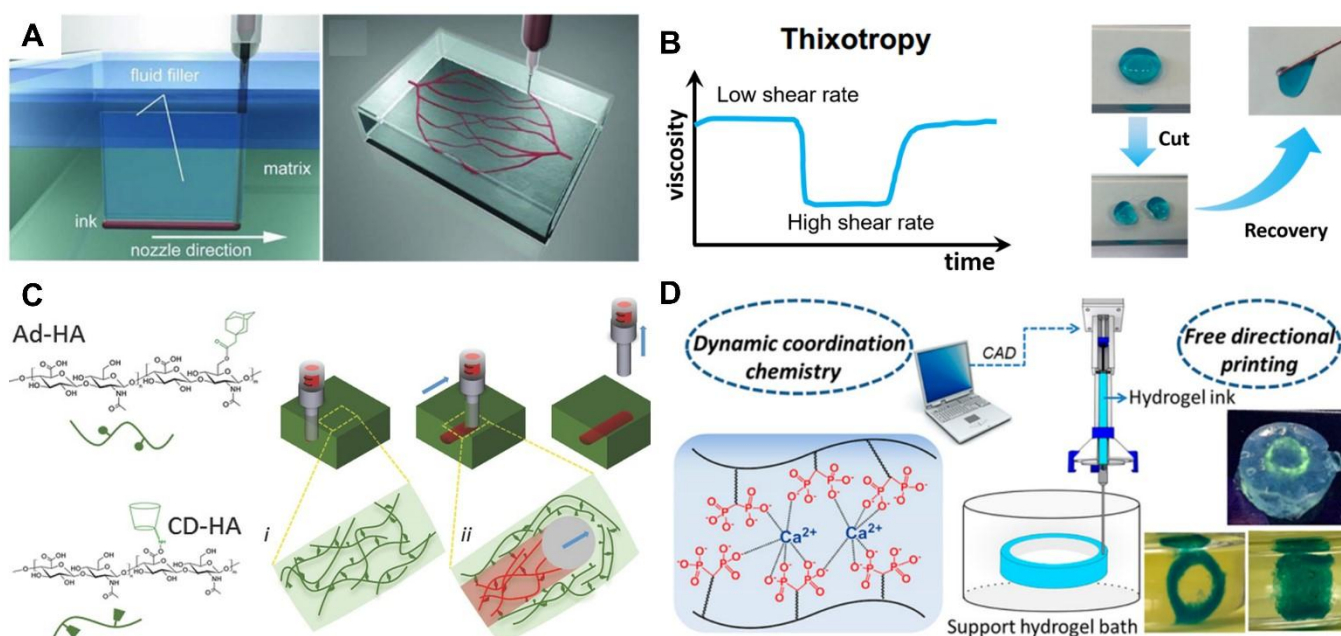


Fig. 1 Bulk gel bath systems with a filler or recovery ability. **A.** Using a filler to fill the crevice during the nozzle movement. left: scheme of the bath system with a fluid filler on the upper surface of the bath matrix; right: a perfusable vascular network was printed using this strategy. Reproduced from Ref. 40 with permission from John Wiley and Sons. **B.** left: a typical viscosity curve of a gel with thixotropic behavior; right: gel with self-recovery ability. Reproduced from Ref. 60 with permission from American Chemical Society. **C.** Bath system based on HA-CD and HA-Ad guest-host interaction. Both the ink and the bath matrix consist of HA-CD and HA-Ad, which give the bath a self-healing ability. The ejected ink can form crosslinking within itself or with the bath matrix. Reproduced from Ref. 58 with permission from John Wiley and Sons. **D.** Bath system based on the metal coordination effect, in which the phosphate groups on polymer chains of ink and calcium ions dissolved in the bath. Reproduced from Ref. 60 with permission from American Chemical Society.

developed a self-healing interpenetrating polymer network (IPN) hydrogel bath consisting of polyethylene glycol (PEG) and alginate. Owing to the fast self-healing ability (within a few seconds) during the print process, they demonstrated printed filaments with a diameter of about 50 μm . Moreover, the constructed fibrin inside their bath (20% PEG - 2.5% alginate) showed not only high resolution but also width consistency

the nozzle is moving in the bath, a velocity gradient field and stress distortion will form around it, which will affect the filament previously printed in this region. Theoretically, the smaller the region, the lower the influence on the previously printed structure. It is, therefore, crucial to understand the relationship between the yield area or velocity distribution and the rheological properties of the bath for optimizing the bath

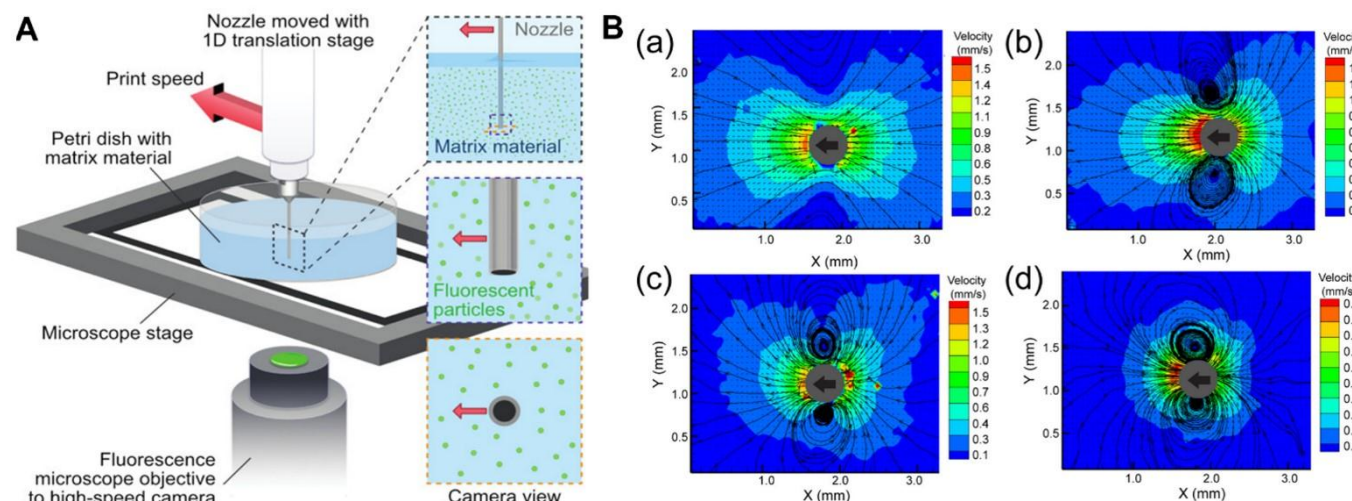


Fig. 2 A. PIV system for visualization of the stress region and velocity field. Particles with fluorescence labels are used to investigate the velocity field. Reproduced from Ref. 54 with permission from American Chemical Society. **B.** The velocity field change of the bath when the nozzle is moving. SE1700 concentration: (a): 33%; (b) 50%; (c) 66% and (d) 80%. With the increase of filler content, the disturbance decreased. Reproduced from Ref. 54 with permission from American Chemical Society.

along its length.

For self-healing gel baths, the printing fidelity and resolution are closely related to the thixotropic recovery time of the polymer gel bath, which is defined as the time taken for the bath to recover its viscosity after the shear stress is released. Since the ejected ink may disperse in the crevices or void caused by nozzle movement before the recovery of the gels and thus lead to morphological change and position deviation of the printed structure, a short recovery time was generally considered to be conducive to the enhancement of printing accuracy.⁶¹ Ideally, the bath can recover immediately after nozzle retraction to trap the extruded ink filament at the programmed position.¹⁴ The thixotropic behavior is usually correlated to the matrix concentration, chemical composition, and shear rate. Generally, the thixotropic properties have been evaluated by rheological measurements or directly observed by particle image velocimetry (PIV). For example, Grosskopf *et al.*⁵⁴ investigated the thixotropic behavior of matrix materials composed of mixtures of PDMS materials (Sylgard 184 and SE 1700, a fumed silica-filled PDMS (approximately 20 wt % fumed silica), depending on concentrations of the SE 1700 (33 wt% - 80 wt%). They showed that with an increase of the SE1700 content from 33 wt% to 80 wt%, the yield stress of the bath was increased and the thixotropic recovery time was significantly reduced from about 2395 s to 16 s.

2.1.3 Stress region and velocity field. The deformation or disturbance of the matrix caused by the nozzle movement is one of the main factors that leads to the displacement of printed features and prevents resolution enhancement. When

design and guiding the high-resolution printing. However, the effect of the distortion field created by nozzle movement on the print quality has rarely been investigated.

PIV is a powerful method of investigating the velocity field and stress distribution around a rigid object in a flowable bath.^{62, 63} Grosskopf *et al.*⁵⁴ used this method to visualize the speed field around the nozzle during its movement process. As shown in **Fig. 2A**, they systematically examined the effect of the rheological behavior and the mechanical modulus of the bath on the resolution of the embedded 3D printing based on polymer bath composed of two types of PDMS, Sylgard 184 and SE 1700 (which contained approximately 20 wt % fumed silica). They found that a significant vorticity region existed near the nozzle and the size of this region was dependent on the τ_y of the bath. The vorticity region became stronger in the matrices with a higher content of fumed silica, which is more elastic (higher G' and higher yield stress) in dynamic conditions. Moreover, exponential decay in velocity in front of the nozzle was observed to be faster with increasing SE 1700 and fumed silica content, while changing the nozzle diameter and speed did not affect the non-dimensional decays (**Fig. 2B**).

The yield region was also evaluated by analyzing the shear rate field in the nozzle movement area. The Oldroyd number (Od), defined as the ratio of τ_y of material to the viscous stresses in a flow, was introduced to analyze the dimension of the yielded area of the bath when a cylindrical nozzle shaft moved through the bath. Od can be calculated as below:

$$Od = \frac{\tau_y d^n}{KU^n} \#(1)$$

where U denotes the movement speed of the nozzle, d refers to the nozzle's outer diameter. K and n are constants, can be determined by the Herschel–Bulkley model.

$$\tau = K\gamma^n + \tau_y, \quad \gamma > \tau_y \#(2)$$

$$\tau = 0, \quad \gamma \leq \tau_y \#(3)$$

Their results indicated that Od and τ_y of matrix are key determinants in controlling the size of the yielded fluid envelope around rigid objects.⁵⁴ Results indicated that a higher Od leads to smaller yielded regions around the nozzle, suggesting that the print fidelity can be increased by increasing Od when a print path is selected that minimizes the previously patterned feature's exposure to the matrix yielding around the translating nozzle.

These insights can guide the optimization of matrix property, inform printing parameter choices, aid print path design, and ultimately allow the fabrication of complex architectures with improved printing fidelity and resolution. However, it should be noted that many of the current conclusions are empirical and established on a single bath material. Due to the differences in bath materials, more detailed factors should be considered.

2.2 Effect of printing parameters on the resolution

The printing parameters can greatly affect the printing resolution. Even in a selected bath system, the variation of printing parameters including the ejection speed, nozzle movement speed, and nozzle size may result in distinct variations in printing accuracy. According to data analysis from past literature, O'Bryan *et al.*⁶¹ ascertained that the printed feature size generally can be predicted from deposition rate (Q) and the nozzle movement speed (v) based on the volume conservation principle (Fig. 3A). Theoretically, the diameter of the printed ink (d_{ink}) can be simply estimated as below, if the shape of the printed ink was an ideal cylinder:

$$d_{ink} = 2 \times \sqrt{\frac{Q}{\pi v}} \#(4)$$

where Q is volume flow rate, and v represents the movement speed of the nozzle in the bath. Thereby, a reduction of Q or an increase of v can basically lead to a decrease of the filament size. For example, Lewis *et al.*^{24,40} reported that the diameter of the filament can be monitored by a dynamic pressure variation approach in which a single nozzle can print different sizes by changing the pressure (i.e. changing the Q) and movement speed. To demonstrate this, they used a glass capillary with a very small diameter (30 μm) to successfully

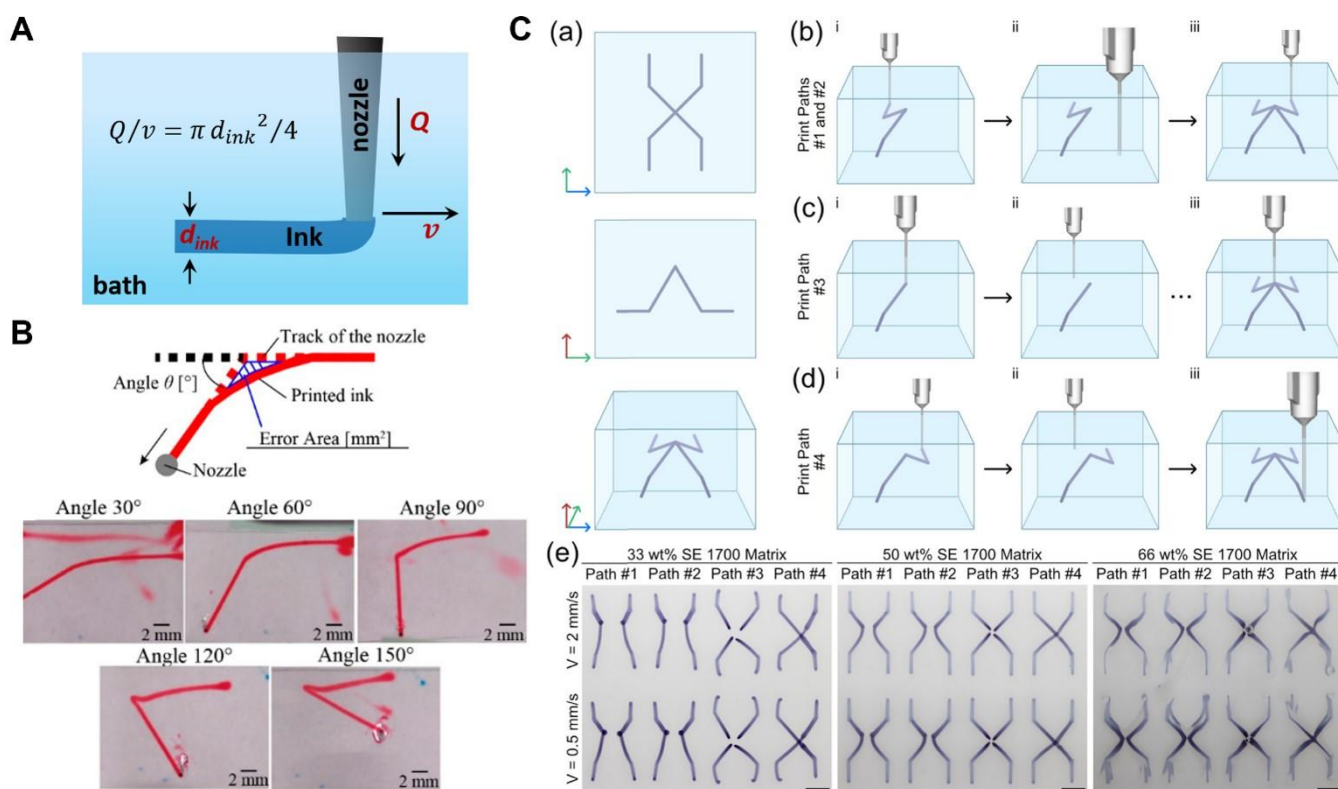


Fig. 3 A. Scheme of the printed ink in a bath. Assuming that the cross-section of the printed ink filament as a circle, the diameter of the printed filament can be calculated from the extrusion speed Q and nozzle movement speed v based on the volume conservation principle. **B.** Designed model corner patterns with a certain angle. The error area increased as the angle θ increased. Reproduced from Ref. 64 with permission from Multidisciplinary Digital Publishing Institute. **C.** Printing sample feature with a different path. (a) Top-down (top), side-on (middle), and 3D (bottom) views of a simple form that is printed. The blue, green, and red arrows to the left represent the X -, Y -, and Z -axes, respectively. (b–d). Schematic illustrations of print paths #1 through #4. For paths #1 and #2, the form is printed in halves: i) left half of the form is printed, and the nozzle is raised out of the matrix and ii) brought to the next start location, and iii) right half of the form is printed. Paths #1 and #2 differ in that in path #2, a 5 min pause in printing is inserted before step ii). (c) For path #3, the form is printed in four segments i) with each segment terminating at the vertex. ii) Printing continues in a clockwise fashion until iii) the last segment is printed. (d) For path #4, the form is printed again in halves, but in a fashion to minimize ink displacement. i) Bottom left and top right segments are first printed in one continuous filament, ii) tip is brought to the next location, and iii) top left and bottom right segments are printed in one continuous filament. (e) Results of printing the form with each print path in 33 wt % (left), 50 wt % (middle), and 66 wt % (right) SE 1700 matrices with each print path are shown for two print speeds, $U = 2$ mm/s (top row) and 0.5 mm/s (bottom row). (Nozzle $d = 0.52$ mm; scale bars = 3 mm.) Reproduced from Ref. 54 with permission from American Chemical Society.

fabricate microchannels with different sizes ranging from 18–170 μm . Likewise, in the research by Burdick *et al.*,⁵⁸ the size of the printed features was controlled by maintaining a constant nozzle movement speed and varying the nozzle types with different inner diameters. Linear supramolecular filaments with diameters including 950, 370, and 35 μm were printed using 20-, 27-, and 34-gauge needles (inner diameter was around 600, 210, and 50 μm), respectively. Here it should be noted that the adjustment of printing parameters cannot reduce the filament size indefinitely since a further reduction of Q or an increase of v will lead to the breakup of the filament.⁴⁰ Moreover, when a small feature is printed in a bath with a small yield stress, the surface tension of the ink may also segment the ink filament into beads if the ink is immiscible with the bath materials.

On the other hand, the printing parameters will also affect the positional reliability of the printed filament. To evaluate the positional accuracy of the ink in the printing process, Uchida *et al.*⁶⁴ printed a series of straight lines with various printing parameters, and different bath conditions, and recorded the positional relationship between the nozzle tracks and filament after ejection. Results showed that the z-position error (the distance between printed ink and nozzle in the ejection direction) of the printed ink increased with increasing ejection speed (V) which was defined with the nozzle diameter d and the volume flow rate (Q) as follows.

$$V = \frac{Q}{\pi\left(\frac{d}{2}\right)^2} \quad \#(5)$$

Besides V , the depth h of the nozzle in the bath would also have an impact on the positional accuracy, probably because the pressure loss occurring at the back of the cylindrical nozzle caused by the nozzle movement differs at different depths in the bath.

The printing route selection has an identical impact on the pattern accuracy of the final printed products. A reasonable printing route design plays an essential role in realizing high-resolution printing. Ideally, the printed filament should be fixed by the bath material to form the intended patterns that are the same as the programmed tracks of the nozzle. However, the ink after printing may be slightly dragged by the nozzle and thus not exactly match the route of the nozzle. The distortion of the ink resulting from the nozzle movement may also lead to a loss of structural fidelity of the printed patterns. For example, Uchida *et al.*⁶⁴ introduced an error area, which was defined as the dragged area of the patterned ink at the corner, to evaluate the location difference caused by filament movement. As shown in **Fig. 3B**, they designed several model corner patterns with different angles. The results showed that the error area increased as the angle increased, reaching a maximum when the angle was 120° for all three nozzle speeds. For all angles, the slower the nozzle speed V , the smaller the error area. According to these results, they suggested that a low flow rate and slow stage speed should be chosen to print a corner pattern precisely. Grosskopf *et al.*⁵⁴ also demonstrated that the path design has a significant influence on the print quality. They designed

different routes to print the same structure under the same conditions. As shown in **Fig. 3C**, the final print quality was clearly different, indicating that the movement of the nozzle may lead to position deviations of filament, suggesting the importance of the path selection for high-fidelity 3D bath-supported printing.

2.3 Effect of the deformation after printing

The morphological change of the ink after printing is an impediment to the fabrication of high-quality construct. The embedded ink materials, especially the soft biomaterial-based gels or solutions, gradually deform in the bath due to certain mechanical or/and chemical interactions with the bath materials.⁶¹ This may lead to a waste of all of the previous efforts made to enhance the resolution and fidelity. The swelling or shrinking driven by osmotic pressure has been a frequently cited reason for the deformation of ink in a bath. For example, Lewis *et al.*²⁴ printed a cell-laden construct in a gelatin methacrylate (GelMA) bulk matrix. They found the printed features swelled in the bath and became twice as large due to the difference in water content between the bath and ink. The intermix between printed ink and bulk materials is another factor that can evidently affect the shape and size of the printed ink. Using a bath that is immiscible with the ink materials is a feasible strategy for preventing the diffusion and mixture between ink and bath, as is reducing the roughness of the filament surface.⁶¹

2.4 Effect of the bio-laden ink

For the cell-laden printing, the cellular proliferation, migration, and scaffold remodeling could gradually change the printed structure,⁶⁵ resulting in the loss of structural fidelity after a period of culture time. For example, Burdick *et al.*⁵⁹ printed a channel structure in a support gel consisting of hyaluronic acid modified with guest-host pairs of adamantane and β -cyclodextrin, and the human umbilical vein endothelial cells (HUVEC) were seeded on the printed channel to mimic a blood vessel. After culturing for 2 days under the stimulus of a gradient of angiogenic growth factors, the sprouting of HUVEC from the channel wall was observed. This phenomenon can be attributed to the protease degradation of the surrounded hydrogel caused by cell growth. Sharma *et al.*⁶⁶ reported that the pluripotent stem cells that incorporated in the fibrin gel-based bioink could degrade the printed gel by proteases, which reduced the structural stability of printed construct, and limited the long-term culture of the sample for cell differentiation. These cell behaviors would lead to a morphological change of the printed filament and loss of printing fidelity. Therefore, in a practical printing process, the unstable deformation behavior of the printed features should be considered.

3. Effect factors in a microgel bath

Compared with the bulk gel bath, the microgel bath has opened a new horizon for supporting 3D bioprinting. In contrast to the bulk gel bath where the whole bath is a single piece of gel, the microgel bath consists of a large number of microgels that are jammed together. The special morphology of the microgel bath prompts a smooth transition between fluid and solid states, and has therefore been regarded recently as an ideal medium for the fabrication of a macroscopic structure with microscopic precision. Theoretically, most gels that can be turned into stable particles with a size in microscale can be used as a bath for printing. Nevertheless, it should be borne in mind that, in practical experiment, the physicochemical properties of the microgels including their size, shape and modulus, flowability, self-healing ability, and biostability may inevitably affect the ultimate printing resolution and structural fidelity.⁶⁷

3.1 Effect of the particle size of a microgel on the resolution

For microgel bath-supported 3D printing, the size of the microgel in the bath matrix is one of the important factors that dictates the printing resolution and fidelity. Since the printed ink filament is in direct contact and interacts with the surrounding microgels after ejection from the nozzle, the size and shape of the microgels usually determine the minimum size of the printing feature. Generally, a bath with a small size and uniform distribution is a prerequisite for improving the printing resolution.⁷ As a typical instance, Hinton *et al.*⁶⁸ reported an innovative method in 2015, called freeform reversible embedding of suspended hydrogel (FRESH), for 3D printing of complex biological structures. This method involved a gelatin microgel slurry as a thermo-reversible and biocompatible support bath. The bath was prepared by blending the gelatin gel into a microgel with an average size of about 65 μm , which allowed for 3D printing of soft biomaterials including alginate, collagen and fibrin with an

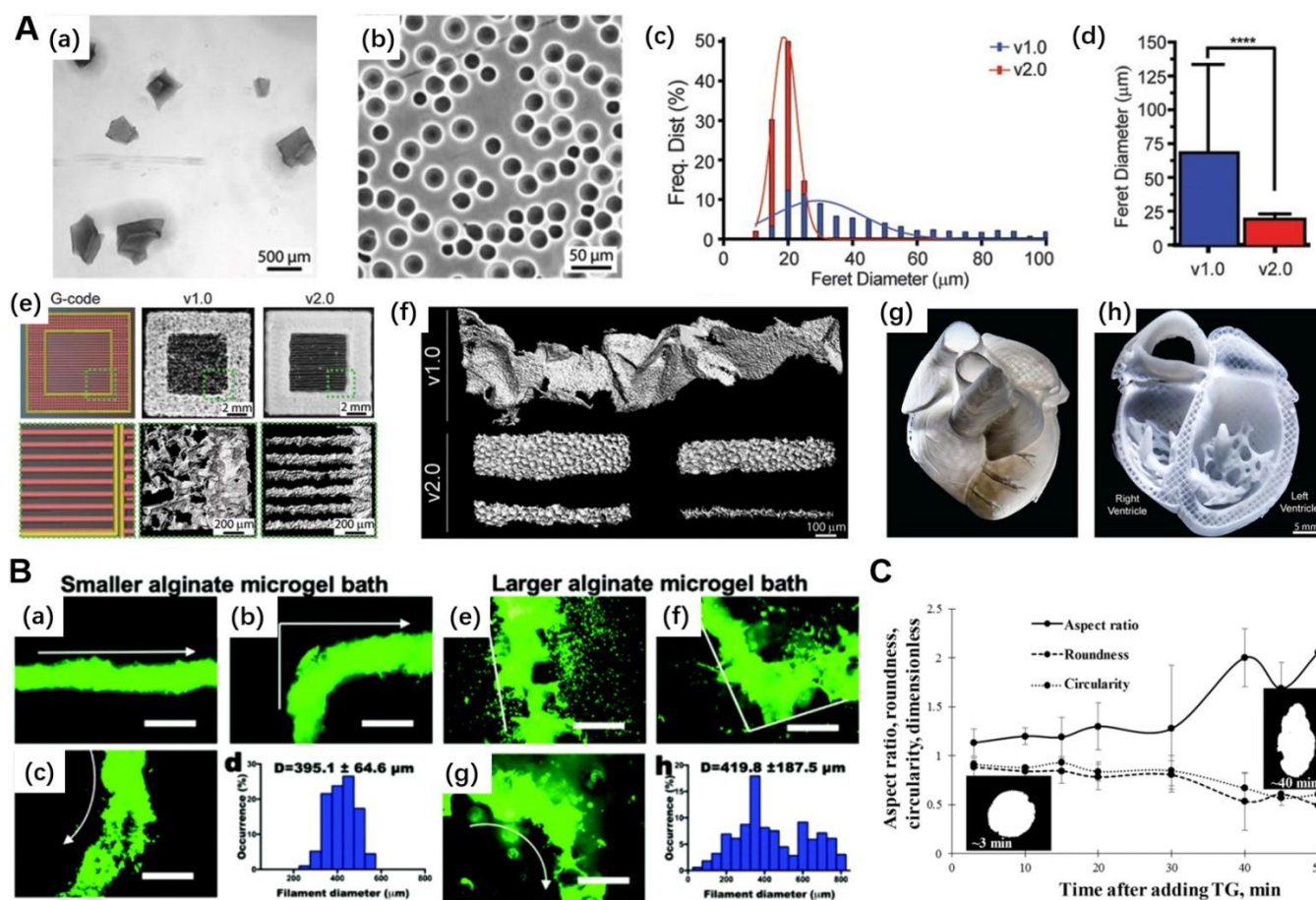


Fig. 4 Size effect of the particle bath. **A.** Freeform reversible embedding of suspended hydrogel (FRESH) method improved by using a smaller particle gel for printing collagen heart with higher resolution. (a–b) Representative images of the gelatin microparticles in the support bath for FRESH v1.0 and v2.0, respectively. (c) Size distribution of the microgels in bath of v1.0 and v2.0 respectively. (d) Average size of microgels. (e) A “window-frame” print construct with single filaments across the middle, comparing G-code (left), FRESH v1.0 (center), and FRESH v2.0 (right). (f) Single filaments of collagen showing the variability of the smallest diameter ($\sim 250 \mu\text{m}$) that can be printed using FRESH v1.0 (top) compared to relatively smooth filaments 20 to 200 μm in diameter using FRESH v2.0 (bottom) (g–h) Outside and Cross-sectional view of the collagen heart printed by FRESH v2.0. Reproduced from Ref. 69 with permission from The American Association for the Advancement of Science. **B.** 3D printing in an alginate microgel bath with different particle sizes. (a–c) Live/dead staining of 3D hMSC filaments bioprinted in a straight line, a corner and a curve with a 22 G needle and (d) their diameter distribution in the smaller alginate microgel supporting medium. (e–g) Live/dead staining of 3D hMSC filaments bioprinted in various configurations with a 22 G needle and (h) their diameter distribution in the larger alginate microgel supporting medium. Arrows indicate the direction of movement of the printing nozzle. Scale bars indicate 600 μm . Smaller alginate microgels lead to higher resolution printing by limiting diffusion of cells into the pores of the microgel bath. Thickness of the cell filaments also are more narrowly distributed in smaller microgel medium. Reproduced from Ref. 70 with permission from The Royal Society of Chemistry. **C.** The aggregation of gellan/gelatin mixture microgels induced by gradual crosslinking of transglutaminase, leading to the reduction of fidelity. Reproduced from Ref. 73 with permission from American Chemical Society.

elastic modulus <500 kPa, but the results indicated that the resolution was only 200 μm . Recently, they developed FRESH v2.0 to exceed the resolution of the previous version (FRESH v1.0).⁶⁹ In this version, they modified the bath preparation method and developed a new bath in which the gelatin microgel had a size that went down to 20 μm . By using this bath, the printing resolution was substantially enhanced and precise printing was realized with an improved resolution of 20 μm , as shown in **Fig. 4A**. Thanks to the enhanced resolution, a human heart was accurately reproduced with patient-specific anatomical structure as determined by micro-computed tomography.^{7,69} Similarly, Jeon *et al.*⁷⁰ recently demonstrated the evident influence of the particle size on the printing resolution by a comparative experiment in which baths containing small and big alginate microgels were used. Here, human bone marrow-derived mesenchymal stem cells (hMSCs) were used as a bioink to generate engineered tissues. Results indicated that the small microgels enabled a higher resolution with narrow filament diameter distribution compared to the larger alginate microgel supporting medium (**Fig. 4B**). The reason for this phenomenon can be attributed to the medium pores that result from the space between the microgels. When the ink is ejected into the microgel bath, it may disperse into the pores or voids between the microgels, leading to a low print precision and broader size of filament than expected. Furthermore, the surface of the filament will become rough and some particle-shaped traps may remain. The ink dispersion was also observed in the FRESH method, in which the printed filament showed visible “spikes” that formed between microparticles.⁶⁸ Since the larger microgels make larger pores and vice versa, printing in a smaller microgel supporting medium can suppress the dispersion of ink and achieve a relatively high printing resolution. However, it should be noted that although the printing precision can be enhanced by reducing the size of the granules, the particle size should be not smaller than 1 μm for the elimination of colloidal scale diffusion.^{67,71,72}

On the other hand, the aggregation of the particles composing the support medium may also impair the print quality. Since high-resolution printing prolongs the working time, this must be considered when considering the size change of the microgels due to aggregation, self-healing, and crosslinking. Ashley *et al.*⁷³ designed a cross-linkable bath by dispersing gellan/gelatin particles in a gelatin solution. Since transglutaminase (TG), an enzymatic crosslinker for gelatin molecules, was added to the bath system, the bath matrix would be gradually crosslinked at ambient temperature. As a result, they observed that the printed channel morphology lost its shape fidelity and gradually shifted from perfectly round to significantly elongated channels after the printing begins for 40 min, as shown in **Fig. 4C**. To restrain the particle aggregation and improve the print quality, Shapira *et al.*⁷⁴ introduced XG as a continuous phase in a calcium-alginate nanoparticles bath. The obtained hybrid bath exhibited smaller particle aggregation and more homogeneous distribution in the bath. To test the effect of aggregation on the printing resolution over time, the alginate microgel bath without the addition of

XG was left to stand for different times before printing. Results showed that a straight filament morphology was formed in the bath with a short standing time, while in the bath which stood for 3 h, an irregular filament was formed. In contrast, the hybrid support could effectively maintain the alignment and accuracy of the printed strands even after a prolonged period. By using this hybrid bath system, they realized high resolutions of down to 10 μm . The inhibition of microgel aggregation in the bath is therefore necessary to achieve high-resolution printing in it.

3.2 Effect of mechanical properties of bath on the resolution

In this section, we also review the mechanical and rheological criteria of microgel baths to accomplish the high-resolution and structural fidelity.

3.2.1 Yield stress. From the perspective of yield stress, an ideal microgel bath should be solid-like in the absence of applied stress, i.e., sufficiently above the critical τ_y to support the printed constructs and prevent the ejected ink from diffusing into the surrounding or sagging because of gravity.^{13,30} Moreover, the bath should have fluent flowability when a nozzle translates in it and rapid recovery once the nozzle moves away from a certain region of the bath.⁷⁵ Unlike the bulk gel with thixotropic characteristics, the deformation of the microgel bath has been accomplished by an unjamming process through the slippage and reconstruction of microgels under the shear stress over τ_y .^{68,76-79} For example, Angelini *et al.*⁶⁷ reported a pioneering work where a granular microgel bath consisting of granular Carbopol gel was used for 3D printing of complex structures through direct writing. PIV observation revealed that the disturbance of the bath caused by the nozzle movement only occurred near the writing tip with about one tip diameter (50 μm in the report), and that the velocity field was not sensitive to the nozzle movement speed. These ideal thixotropic behaviors mitigated the distortion of the bath during the printing process, which facilitated the printing of a complex 3D structure with a high aspect ratio.

The morphology of the printed filament is closely correlated to the yield stress of both bath and ink materials. To prevent the breakup of printed structures driven by interfacial instabilities, the stresses generated by interfacial tension must be less than the τ_y of the microgel.⁸⁰⁻⁸² Based on these criteria, O'Bryan *et al.*⁸² proposed that the minimum stable printed feature size can be predicted to some extent by the microgel yield stress based on postcapillary length (λ), which is defined by the following equation.

$$\lambda = \frac{\gamma}{\tau_y} \#(6)$$

Here, γ was the interfacial tension between bath and ink. To test this relationship, they printed a series of features using silicone oil in micro-organogel baths with different yield stresses, and it was shown that the minimum stable feature size decreases with increasing yield stress, as predicted. Recently, they⁸³ investigated the empirical relationship between yield stress and critical diameter of printed filament by considering a fluid beam embedded within an elastic

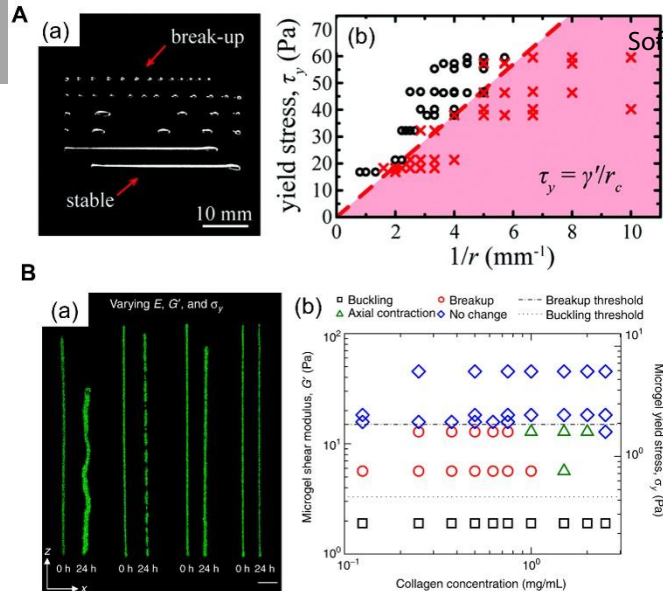


Fig. 5 A. (a) Images of beams printed in packed microgels with yield stress τ_y . Beams with radii smaller than the critical radius break-up into smaller droplets. (b) Stability state diagrams of neat mineral oil beams printed into aqueous microgel supports show the transition from the stable (black) to break-up (red) regimes. Reproduced from Ref. 83 with permission from The Royal Society of Chemistry. **B.** (a) The deformation of beams in packed polyacrylamide bath. By varying the shear modulus of the surrounding microgel medium, G' , and the beam elastic modulus, E , a cascade of different behaviors was observed: the cell-ECM microbeams buckle, breakup, contract axially, and remain stationary. (left to right: collagen $E = 0.035$ Pa and microgel $G' = 1.92$ Pa; $E = 0.1$ Pa, and $G' = 5.69$ Pa; $E = 1$ Pa and $G' = 10.85$ Pa; $E = 0.3$ Pa and $G' = 55.02$ Pa. Scale bar: 1 mm). (b) A two-dimensional map of these behaviors illustrates where transitions occur. (In this case the yield stress and the modulus of bath follow a relationship: $\sigma_y = 0.13 G'$.) The Dotted line indicates G' at breakup and dashed line indicates σ_y at fracture. Reproduced from Ref. 37 with permission from Springer Nature.

support medium. They confirmed that for the microgel bath with yield stress τ_y , there is a critical feature size necessary for the printed ink to remain stable. As shown in **Fig. 5A**, the printed filament with a diameter smaller than the critical radius will break up into smaller droplets due to the capillary force acting at the interface. Morley *et al.*³⁷ investigated the deformation of cell-laden collagen beams printed in aqueous polyacrylamide microgel baths. By monitoring the shear modulus of the surrounding microgel medium, G' , and the beam elastic modulus, E , a cascade of different behaviors including the buckle, breakup, contract axially, and remain stationary were observed, as illustrated in **Fig. 5B**. According to their theoretical analysis and experimental dates, the yield stress of bath material could substantially affect the shape stability of the printed beams that containing cells. They found a threshold yield stress of bath (1.95 Pa for their case) independent with the ink concentration. The microbeams printed in bath with the yield stress higher than this threshold remain stable, straight, and intact, while in the bath with lower yield stress the printed beams would deform due to the internal stress built up within the ink.

In fact, the yield stress can be effectively tuned by adjusting the polymer concentration when preparing the microgel of the bath. Ning *et al.*³¹ used a Carbopol microgel as a bath and reported that the increase of Carbopol concentration led to a larger yield stress of the bath. This resulted in a decrease of the filament diameter and was thus

capable of retaining the strand geometry post-extrusion. Likewise, O'Bryan *et al.*⁸⁴ compared the print quality of four kinds of commercially available microgels with distinct chemical properties. They confirmed that the yield stress of these materials could be tuned by simply changing the polymer concentration of the microgel. For all four kinds of polymer microgel bath, the τ_y at the condition that was favorable for 3D printing ranged from 7 to 10 Pa. With suitable printing conditions, a printing precision as high as 20 μm could be realized using these four commercial microgels as a bath. These results demonstrated that a suitable τ_y is essential for high-resolution printing, and that even commercially available microgels with different chemical properties can be successfully used as bath materials for high-precision 3D printing after optimizing the rheological properties.⁸⁴

3.2.2 Recovery time. The rheological recovery time is an essential indicator for evaluating the recoverability of the bath, which can evidently affect the final printing resolution. It is usually defined as the time needed for the bath to recover its initial mechanical and rheological properties after removal of shearing stress. Ideally, the microgel bath should be capable of spontaneously closing the potential crevices when the hydrostatic stress at the bottom of the crevices exceeds the τ_y of the bath, thereby allowing high-precision 3D printing without using a filler solution.⁶⁷ Currently reported bath materials used for high-resolution 3D printing generally show a recovery time of several seconds. For example, all the commercial microgels in O'Bryan *et al.*'s work⁸⁴ showed short recovery times (about 1 s) at the optimized condition suitable for 3D printing. Such a rapid recovery of the mechanical properties ensures that the ejected ink is quickly encapsulated without remaining crevices or bubbles.^{30, 75, 82} Similarly, to ensure print quality, the alginate microgel bath in the work of Jeon *et al.*⁷⁰ exhibited a rapid recovery of the storage modulus and viscosity to their initial values within seconds. In fact, the recovery time depends on the mechanical properties of microgels and can also be tuned by changing the polymer concentration. Increasing the bath concentration facilitates the reduction of recovery time, resulting in the elimination of the crevices or voids formed by nozzle movement. Shapira *et al.*⁷⁴ investigated printing performance using Carbopol microgel as a bath. When the concentration of Carbopol solution increased from 0.1% to 0.2%, the bath exhibited an evident limited recovery time, indicating its ability to rapidly recover.

3.2.3 Viscosity. Besides the yield stress and the thixotropic recovery time, the viscosity of the bath has been reported to affect the print quality. Moxon *et al.*⁷⁵ investigated the influence of supporting matrix viscosity on the printing resolution. It was found that increasing the viscosity of the supporting medium could result in a monotonic increase in resolution in the XY dimensions, but interestingly a smaller reduction in resolution in the Z dimension.⁸² The experimental results of O'Bryan *et al.*⁸² using an organic microgel bath also indicated that an increase of the viscosity of the ink could delay the breakup of unstable features and remarkably enhance the printing resolution from 80 μm to 30 μm . The improvement of viscosity can be realized by enhancing the

polymer concentration of the microgel or increasing the particle density. Ning *et al.*³¹ reported that a higher concentration of Carbopol microgel and denser granular particles in the bath was more conducive to preserving high printing fidelity, especially for printing low-viscosity hydrogel bioinks. This was because the microgel bath with low concentration showed limited mechanical support to soft ink, and the extruded ink could be dragged by nozzle movement to lose its designed position. Moreover, denser particles added to the bath could reduce the gaps between particles and mitigate the infiltration of ink, thereby resulting in a more uniform ink filament. However, there is an optimal range for bath concentration, beyond which the higher microgel concentration may impede the fluency of the nozzle and result in diminished printed fidelity.³¹ On the other hand, increasing the ink viscosity can also be helpful for printing precision and filament integrity, though this ink usually needs a higher extrusion force, which leads to high shear stresses that hamper cell survival for some cell-laden 3D printing.^{31, 84-86}

More details about the rheology of the extrusion-based bioprinting in a suspension bath may be found in a recent review by Cooke *et al.*⁸⁷ They provided an overview of the important rheological parameters for bioink and the methods to assess printability, as well as the effect of bioink rheology on cell viability.

3.3 Effect of printing parameters on the resolution

The printing parameters including the nozzle diameter, ejection rate, and movement speed have key roles in the determination of the printing resolution in a microgel bath. Although the influence of printing parameters on printing resolution is fundamentally similar to that of a bulk gel bath described in the previous section, the size and shape of nozzles are major factors determining the resolution in microgel baths. It can be easily understood that the use of a smaller nozzle leads to higher printing precision.⁴⁹⁻⁷⁰ Shapira *et al.*⁷⁴ realized the printing of filaments with very fine diameters down to 10 μm by using pulled glass pipettes in their optimized bath. Although a finer filament can be achieved by using smaller needle, it may not be suitable for cell printing since most cells are bigger than 10 μm and the high shear stress may rupture them.⁷⁴ Moreover, when some composites ink that containing inorganic particles was used for printing, a fine nozzle may be blocked by the particle aggregations. To overcome this limitation, Chen *et al.*⁸⁸ developed an *in situ* precipitation strategy for 3D freeform printing of inorganic particles-loaded hydrogel construct. Different from the conventional printing using the composite ink premixed with the inorganic particles, this method allows to *in situ* generate nanoparticles during the printing process. By his method, they successfully fabricated hyaluronic acid-alginate/calcium phosphate nanocomposite hydrogel scaffolds with various mineral contents and good structural integrity. The shape of the nozzle is also important for 3D printing with good fidelity, especially for printing complex structures such as vascular networks and hollow heart. For example, to print a continuous helical pattern without damaging the printed structure during the nozzle

movement, O'Bryan *et al.* used a bent nozzle oriented at 45° from vertical to reduce the interruption of nozzle translation.⁸⁴ To investigate the effects of various printing parameters on print quality, the printing optimization index (POI)⁸⁹ was introduced by Lewicki *et al.*⁹⁰ in their work for quantitatively evaluating the printing accuracy. The normalized POI is a dimensionless score ranging from 0 to 1, where 0 is the worst and 1 represents the best resolution. Their work indicated that the printing speed and pressure are important for high resolution, and they pinpointed the optimal conditions under the guidance of POI analysis for printing cells in a sodium alginate microgel bath. Other studies⁷⁴ have also reported that the diameters of a printed filament can be adjusted to some extent, by applying different printing speeds and ink feed speed. Normally, the increase in nozzle movement speed and the reduction of the pressure for ejection of ink result in a finer filament. The resolution improvement by adjusting the printing parameters has a trade-off relationship with the mechanical and rheological properties of baths and inks. For high-resolution 3D printing therefore, the configuration design of a gel-supported 3D printing requires the concurrent consideration of bath, ink and printing parameters.

3.4 Effect factors in Cell-involved Bioprinting

To mimic the native organs consisting of living cells, considerable advances^{45, 91-95} have been reported in bioprinting with cell-containing inks or baths. Besides the resolution determinants mentioned above, the cells or cell aggregates such as cellular spheroid, tissue strand, and organoids in the printing system also have an impact on the printing precision. Firstly, the addition of cells in ink would substantially affect the printability as it can alter the rheological properties of the hydrogel, changing the parameters required for proper extrusion.⁹⁶ Lewicki, *et al.*⁹⁰ used sodium alginate (SA) to creating constructs populated with human neuroblastoma cells SK-N-BE(2) in a gelatin microgel bath by the FRESH method. Their results indicated a notable difference between optimal parameters for printing SA with and without cells. Furthermore, the cell-generated force caused by the cell-cell or cell-gel interaction would also deform the printed product. To investigate the deformation of the 3D bioprinted structures under cell-generated forces, Morley *et al.*³⁷ printed a bioink containing pancreatic cancer cells into a 3D culture medium made from the polyacrylamide microgels. By varying the mechanical properties of the printed beams and the surrounding microgel medium, they observed the buckling, axial contraction, failure, and static stability of the printed beams under cell-generated forces. On the other hand, the cell culture conditions after printing may lead to the swelling, dissolution, or degradation of the biomaterials in the printed structure. As a typical instance, for the alginate gel-based printing, the presence of ions such as sodium ions or magnesium ions may lead to the calcium release from the ionic crosslinked alginate gel and cause its swelling or even dissolution⁹⁷, which was fatal for the structural accuracy of the printed sample. However, if the swelling behavior of the

printed tissue can be controlled, it may be a useful characteristic for generating smart tissues. Lee *et al.*⁹⁸ developed a 4D cellular printing strategy to construct the high cell density tissue using two biodegradable materials. By reasonably tuning the spatial patterning of these two biomaterials with different swelling ratios, the controllable geometric change of the printed construct over time can be realized.

Different from the scaffold-based cellular bioprinting (i.e., cells dispersed within biocompatible materials or decellularized matrix components), the scaffold-free bioprinting using cell aggregates such as cellular spheroid,^{38, 99} tissue strand^{100, 101}, and organoids²³ allows us to fabricate real organ-like structures that have high cell concentration.¹⁰² For example, Bulanova *et al.*¹⁰³ printed a thyroid gland construct using two types of rounded embryonic tissue spheroids, thyroid spheroids, and allantoic spheroids, within the collagen hydrogel. After culture for 4 days, the tissue spheroids fused into a single and integral thyroid gland construct. Moreover, they demonstrated that the printed construct is functional after grafting under the kidney capsule of hypothyroid mice. Skylar-Scott *et al.*²³ also reported the fabrication of living tissue with organ building blocks (OBB) composed of patient-specific-induced pluripotent stem cell-derived organoids. They prepared a cellular matrix by assembling hundreds of thousands of the OBBs, and then the vascular channels were introduced into the matrix via embedded three-dimensional bioprinting. By this strategy, a perfusable cardiac tissue that fuses and beats synchronously over 7 days was successfully created. Despite these encouraging advances, the resolution of bioprinting using cell spheroids is limited by the original size and shape of the cellular assemblies. For example, the reported tissue spheroid usually has a diameter over 100 μm .¹⁰⁴ Moreover, the positional precision of the deposited spheroid is difficult to control by conventional extrusion printing, which will inevitably depress the final printing resolution. To improve the positional precision of the tissue spheroid, Ozbolat *et al.*^{104, 105} developed an aspiration-assisted bioprinting method, by which the positional precision can be enhanced about 11 % with respect to the spheroid size. Considering that the common cell spheroids usually have a diameter range of 80-1000 μm , the high-resolution printing based on cell spheroid is still a challenge. Recently, Jeon *et al.*⁷⁰ created a cell printing platform that permits 3D printing and long-term culture of the individual cell-only bioink within an oxidized and methacrylated alginate microgel supporting bath. Unlike previous 3D bioprinting techniques which depend on external solid materials for structural maintenance or additional process for prefabrication of cell aggregates, this method provided a pathway to generate biomimetic cellular condensation-based engineered tissues with defined geometries. Nevertheless, the currently achievable resolution of this cell-only bioprinting is around 160 μm , which is still far away from the structure resolution of real-tissue. Therefore, to create reproducible and useful models by bioprinting *in vitro*, more efforts focusing on the printing precision are still demanding.

Conclusions and future directions

Bath-supported 3D bioprinting has rapidly developed in the last half decade and a considerable number of bath systems have been designed and used for bio-applications (as shown in **Tables 1 and 2**). This review focused on the printing resolution of various bath systems and comprehensively introduced the factors that affect the printing resolution and fidelity when printing in bulk polymer solution baths and granular microgel baths, respectively. In particular, the influences of the mechanical and rheological characteristics of both bulk polymer and microgel baths on the printing precision were discussed. The relationship between the detailed parameters during the printing process and the printing fidelity was also summarized. Moreover, the factors possibly determining the precision of printed features after printing were analyzed. In each aspect, the influence pattern and its mechanism were identified based on existing research reports and relevant theories.

For a bulk gel bath, the resolution greatly depends on its rheological properties. An ideal bath should have suitable yield stress that not only allows the smooth movement of the nozzle within it but also supports and fixes the ejected ink. A bath with a yield stress one order higher than that of the ink material is recommended. Moreover, the bulk gel used for high-resolution printing requires a rapid thixotropic recovery time, usually under a few seconds. The rheological properties can be adjusted by changing factors such as the polymer concentration, filler content, and intermolecular interaction, etc. In terms of the printing parameters, the printing resolution is closely related to the extrusion speed and nozzle movement speed, as they directly affect the diameter of the printed filament. Generally, a faster movement speed leads to a thinner filament. An over-fast movement speed, however, may cause the printed filament to break and have a negative influence on the resolution. Besides, a reasonable printing path should be considered to mitigate the distortion of the printed structure by the movement of the needle. Finally, the shrinkage/swelling of the printed structure in a bath and deformation caused by cell migration in cell-laden printing need to be taken into account when conducting high-precision 3D printing.

For a microgel bath, the particle size and distribution have a significant impact on the printing resolution. In principle, a smaller particle size and uniform size distribution facilitate the improvement of resolution. It should be noted however that the particle size should be not smaller than 1 μm for the elimination of colloidal scale diffusion. Moreover, the aggregation or swelling of gels in the bath should be avoided during the printing process to ensure a reliable printing result. Theoretically, most gels that can be turned into stable particles with a size in microscale can be used as a bath for printing. For high-resolution printing, certain rheological properties including suitable yield stress and rapid recovery behavior are also required. Other effect factors such as the printing parameters and path design are similar to the rules for bulk gel baths.

To print 3D structures with high resolution and feature fidelity, suitable bath characteristics and optimal printing parameters are the prerequisites. Although it is difficult to get a universal selection rule, the empirical criteria summarized from the literature and rules outlined in this review offer guidance and reference for bath design and the selection of printing parameters for future studies in high-precision, bath-supported 3D bioprinting.

In truth, current 3D printing technology cannot realistically duplicate organs or tissues with an *in-vivo*-like structure and biological function. However, there is no doubt that 3D bioprinting, especially bath-supported 3D printing, has evolved markedly and become an increasingly important tool in bio-applications such as tissue engineering and organ model reconstruction. Currently, the optimal resolution of 10 μm can be realized using bath-supported 3D printing.⁷⁴ This precision can basically permit the fabrication of 3D cell-resolution structures. The resolution below 10 μm is barely reported in the extrusion-based bioprinting. This is probably because: (1) The nozzle size cannot be infinitely reduced. The nozzle with very small inner diameter is easy to be blocked or broken, which is inconducive to the sustainable and continuous printing. (2) The printed filament with a submicron diameter is not stable and may break up into smaller droplets in bath due to the capillary force acting at the interface. (3) The size of a single mammalian cell is usually ranging from 10 to 100 μm . The cell-laden bioprinting therefore usually showed resolution bigger than 10 μm .

Despite the encouraging advances achieved recently, the current state of bath-supported 3D bioprinting is still confronted with many obstacles. First, there is a conflict between printing precision and printing time. It is known that the enhancement of printing resolution generally results in an increase of the total number of printing layers to print the same volume and requires a longer printing time. However, for most 3D bioprinting platforms, the mechanical or rheological properties of the bath and ink may change during the long printing duration.^{12, 106} Moreover, for cell-involved 3D bioprinting, the viability of cells is difficult to maintain over a long period under these printing conditions. Both factors hinder the practical applications of 3D bioprinting. Therefore, when printing a large-scale product like organs, the combination of high resolution and low resolution during the printing process may be a possible compromise for timesaving. For example, Mirdamadi *et al.*¹⁰⁷ recently 3D printed a full-size heart model using the FRESH method, and they chose a small size nozzle to ensure the resolution of some small constructs, while using a large size nozzle to print the main part of the model to balance the precision and printing duration. To further improve the printing effectiveness in future experiments, multi-nozzle printing is a potential alternative.^{108,}

¹⁰⁹ Bio-printing with multiple dispensing heads enables the simultaneous printing of different parts of the intended structure with separated ink materials, which could remarkably shorten the printing time without losing precision.¹¹⁰⁻¹¹³

Second, for most bath-supported 3D printing, the matrix materials attached to the printed structures will inevitably diminish the final resolution. Although many bath materials enable high-resolution printing, removing them after printing is difficult.¹¹⁴ The attached materials on the printed object may alter the size and structural fidelity of the product, thereby hindering it with undesirable functions. Therefore, the printed object must be released from the bath when the printing is finished. Current methods for removing the attached matrix generally involve post-processing such as thermal melting, dissolution, targeted washing, and sonication.^{68, 115} However, the complete removal of the attached gels on the bioproduct still has some limitations. For example, thermal treatment for melting the bath may be useless for removing the bath pieces that were encapsulated inner the printed structure. The dissolution of a gel bath requires multiple solution exchange steps with a large amount of solvent, which is not only costly but may also lead to the swelling of some hydrated products.¹¹⁴ Other methods such as sonication or chemical degradation are limited since the bioproducts, especially the cell-containing product, are usually sensitive to mechanical stress, heat, pH, and many organic chemicals. This limitation makes it clear that improvements in gel-supported 3D printing in terms of bath removal will be necessary in the future.

Third, the printing resolution and fidelity are affected by the accuracy and reliability of the printer, but at present, a standard platform for manufacturing and operation of a commercial 3D printer is still lacking. Studies vary as they are usually based on printers provided by different companies or even homemade or laboratory-modified machines.^{13, 116-118} This is an obstacle to inter-study comparison of the effects of detailed printing parameters on the print quality. With the continuous development of 3D printing technology, we believe relevant standards will be gradually improved through the cooperation of scientific researchers and mechanical engineers.

Overall, bath-supported 3D bioprinting as an emerging technology has rapidly developed in the past few years. To date, novel printing strategies have been demonstrated with printing resolutions from 1,000 μm to 10 μm . Since the printing resolution is affected by many factors, thorough consideration of the balance of these factors is imperative for high-precision 3D printing. We hope that by bridging the effect factors in the printing process with the printing resolution, this review will provide inspiration to those who intend to use gel-supported 3D printing.

Table1 Printing resolution of recent research in bulk gel bath

Resolution range (μm)	Bath	Ink	Resolution* (μm)	Year [ref]
------------------------------------	------	-----	-------------------------------	------------

ARTICLE			Journal Name
< 100	HA-Ad and HA-CD Guest-host bath	Cell-containing guest–host complexes	2015 ⁵⁸
	Pluronic F 127-CaCl ₂	alginate	2018 ⁵
100 ~ 300	Carbopol gel	PDMS prepolymer	2016 ¹¹⁹
	Pluronic F127 diacrylate	Pluronic F127	2011 ⁴⁰
	Gelatin-CaCl ₂	gold nanorod incorporated GelMA	2017 ¹²⁰
	PEG/alginate/ thrombin	hMSCs spheroids-laden fibrinogen	2019 ³⁸
	xanthan-gum	alginate	2020 ³⁹
> 300 or no date	bisphosphonate-functionalized hyaluronic acid	bisphosphonate-functionalized hyaluronic acid	2017 ⁶⁰
	mixing of CD-HA and AdNor-HA	mixing of Ad-HA and CD-HA	2018 ⁵⁹

* Resolution is estimated from the minimum diameter of the printed filament.

Table 2 Printing resolution of recent research in microgel bath

Resolution range (μm)	Bath	Ink	Resolution* (μm)	Year [ref]
< 100	calcium-alginate nanoparticles and xanthan gum	pepsinized collagen-based hydrogel	10	2020 ⁷⁴
	Gelatin microgels	collagen	20	2019 ⁶⁹
	Pemulen TR-2NF microgel (commercial)	PVA	20	2018 ⁸⁴
	SEP and SEBS block copolymer micro-organogel	Silicone elastomer	80	2017 ⁸²
100 ~ 300	Carbopol microgels	PVA and other polymers	100	2015 ⁶⁷
	Carbopol	gelMA	200	2020 ³¹
	Granular Carbopol ETD 2020	Cell cluster	200	2016 ³⁶
	Organ building blocks	gelatin	200	2019 ²³
	Carbopol (ETD 2020)	Alginate and gelatin	>200	2016 ¹²¹
	Gelatin microgels slurry	Alginate; Collagen (I); ECM	~250	2015 ⁶⁸
	Fluid agarose gel	Cell-loaded gellan	250	2017 ⁷⁵
> 300 or no date	Gellan gum microgels	Gelatin based composites	>300	2019 ¹¹⁴
	alginate microgel	hMSCs cells	200-800	2019 ⁷⁰
	Alginate granules+ Xanthan	Cy5-prestained CMs or RFP-	<300	2019 ⁴⁵

gum	expressing ECs		
Gelatin-Gellan Microgel Composite	alginate	750-1000	2020 ⁷³
gelatin granules	hSKMs in dECM	300-1000	2019 ²⁵
gelatin slurry	cell-laden alginate microgel	-	2019 ⁹¹

* Resolution is estimated from the minimum diameter of the printed filament.

Author Contributions

Zheng-Tian Xie: Literature search and investigation, writing - original draft, writing - review & editing. **Dong-Hee Kang:** Literature search and investigation, writing -review & editing. **Matsusaki Michiya:** Supervision, writing - review & editing, funding acquisition.

Conflicts of interest

There are no conflicts to declare.

Acknowledgements

The authors acknowledge financial supports by Mirai-Program (18077228) from JST and Grant-in-Aid for Scientific Research (A) (20H00665) from JSPS and Bilateral project between JSPS and DAAD (JPJSBP120213505).

Notes and references

- Z. Gu, J. Fu, H. Lin and Y. He, *Asian J Pharm Sci*, 2020, **15**, 529-557.
- R. L. Truby and J. A. Lewis, *Nature*, 2016, **540**, 371-378.
- W. Zhu, X. Ma, M. Gou, D. Mei, K. Zhang and S. Chen, *Curr. Opin. Biotechnol.*, 2016, **40**, 103-112.
- A. W. Feinberg and J. S. Miller, *MRS Bull.*, 2017, **42**, 557-562.
- M. Rocca, A. Fragasso, W. Liu, M. A. Heinrich and Y. S. Zhang, *SLAS Technol*, 2018, **23**, 154-163.
- F. Momeni, S. M. Mehdi Hassani, X. Liu and J. Ni, *Materials & Design*, 2017, **122**, 42-79.
- D. C. Corbett, E. Olszewski and K. Stevens, *Trends Biotechnol.*, 2019, **37**, 1153-1155.
- M. E. Prendergast and J. A. Burdick, *Adv. Mater.*, 2020, **32**, e1902516.
- P. Datta, M. Dey, Z. Ataie, D. Unutmaz and I. T. Ozbolat, *npj Precision Oncology*, 2020, **4**.
- K. Karzyński, K. Kosowska, F. Ambrozkiewicz, A. Berman, J. Cichoń, M. Klak, M. Serwańska-Swiętek and M. Wszola, *Medical Studies*, 2018, **34**, 93-97.
- M. Farsari and B. N. J. N. p. Chichkov, 2009, **3**, 450-452.
- A. K. Miri, I. Mirzaee, S. Hassan, S. Mesbah Oskui, D. Nieto, A. Khademhosseini and Y. S. Zhang, *Lab Chip*, 2019, **19**, 2019-2037.
- T. Jiang, J. G. Munguia-Lopez, S. Flores-Torres, J. Kort-Mascort and J. M. Kinsella, *Applied Physics Reviews*, 2019, **6**.
- S. Chen, W. S. Tan, M. A. Bin Juhari, Q. Shi, X. S. Cheng, W. L. Chan and J. Song, *Biomed Eng Lett*, 2020, **10**, 453-479.
- W. Sun, S. Schaffer, K. Dai, L. Yao, A. Feinberg and V. Webster-Wood, *Front Robot AI*, 2021, **8**, 673533.
- R. E. Saunders, J. E. Gough and B. J. B. Derby, 2008, **29**, 193-203.
- T. Xu, J. Jin, C. Gregory, J. J. Hickman and T. J. B. Boland, 2005, **26**, 93-99.
- V. Mironov, R. P. Visconti, V. Kasyanov, G. Forgacs, C. J. Drake and R. R. J. B. Markwald, 2009, **30**, 2164-2174.
- M. Gruene, A. Deiwick, L. Koch, S. Schlie, C. Unger, N. Hofmann, I. Bernemann, B. Glasmacher and B. J. T. E. P. C. M. Chichkov, 2011, **17**, 79-87.
- N. R. Schiele, D. T. Corr, Y. Huang, N. A. Raof, Y. Xie and D. B. J. B. Chrisey, 2010, **2**, 032001.
- A. P. Zhang, X. Qu, P. Soman, K. C. Hribar, J. W. Lee, S. Chen and S. J. A. m. He, 2012, **24**, 4266-4270.
- D. Ahn, L. M. Stevens, K. Zhou and Z. A. Page, *ACS Cent Sci*, 2020, **6**, 1555-1563.
- M. A. Skylar-Scott, S. G. M. Uzel, L. L. Nam, J. H. Ahrens, R. L. Truby, S. Damaraju and J. A. Lewis, *Sci Adv*, 2019, **5**, eaaw2459.
- D. B. Kolesky, R. L. Truby, A. S. Gladman, T. A. Busbee, K. A. Homan and J. A. Lewis, *Adv. Mater.*, 2014, **26**, 3124-3130.
- Y. J. Choi, Y. J. Jun, D. Y. Kim, H. G. Yi, S. H. Chae, J. Kang, J. Lee, G. Gao, J. S. Kong, J. Jang, W. K. Chung, J. W. Rhie and D. W. Cho, *Biomaterials*, 2019, **206**, 160-169.
- M. A. Skylar-Scott, S. G. Uzel, L. L. Nam, J. H. Ahrens, R. L. Truby, S. Damaraju and J. A. J. S. a. Lewis, 2019, **5**, eaaw2459.
- R. Landers, U. Hübner, R. Schmelzeisen and R. J. B. Mülhaupt, 2002, **23**, 4437-4447.
- I. T. Ozbolat and M. J. B. Hospodiuk, 2016, **76**, 321-343.
- C. Colosi, S. R. Shin, V. Manoharan, S. Massa, M. Costantini, A. Barbetta, M. R. Dokmeci, M. Dentini and A. J. A. m. Khademhosseini, 2016, **28**, 677-684.
- A. McCormack, C. B. Highley, N. R. Leslie and F. P. W. Melchels, *Trends Biotechnol.*, 2020, **38**, 584-593.
- L. Ning, R. Mehta, C. Cao, A. Theus, M. Tomov, N. Zhu, E. R. Weeks, H. Bauser-Heaton and V. Serpooshan, *ACS Appl Mater Interfaces*, 2020, **12**, 44563-44577.
- C. B. Highley, K. H. Song, A. C. Daly and J. A. Burdick, *Adv Sci (Weinh)*, 2019, **6**, 1801076.
- H. Park and K. Park, *ACS Sym Ser*, 1996, **627**, 2-10.
- E. M. Ahmed, *J Adv Res*, 2015, **6**, 105-121.
- D. L. Taylor and M. In Het Panhuis, *Adv. Mater.*, 2016, **28**, 9060-9093.

36. T. Bhattacharjee, C. J. Gil, S. L. Marshall, J. M. Uruena, C. S. O'Bryan, M. Carstens, B. Keselowsky, G. D. Palmer, S. Ghivizzani, C. P. Gibbs, W. G. Sawyer and T. E. Angelini, *ACS Biomater Sci Eng*, 2016, **2**, 1787-1795.
37. C. D. Morley, S. T. Ellison, T. Bhattacharjee, C. S. O'Bryan, Y. Zhang, K. F. Smith, C. P. Kabb, M. Sebastian, G. L. Moore, K. D. Schulze, S. Niemi, W. G. Sawyer, D. D. Tran, D. A. Mitchell, B. S. Sumerlin, C. T. Flores and T. E. Angelini, *Nat Commun*, 2019, **10**, 3029.
38. B. A. G. Melo, Y. A. Jodat, S. Mehrotra, M. A. Calabrese, T. Kamperman, B. B. Mandal, M. H. A. Santana, E. Alsberg, J. Leijten and S. R. Shin, *Adv. Funct. Mater.*, 2019, **29**.
39. S. G. Patricio, L. R. Sousa, T. R. Correia, V. M. Gaspar, L. S. Pires, J. L. Luis, J. M. Oliveira and J. F. Mano, *Biofabrication*, 2020, **12**, 035017.
40. W. Wu, A. DeConinck and J. A. Lewis, *Adv. Mater.*, 2011, **23**, H178-183.
41. G. Štumberger and B. J. M. Vihar, 2018, **11**, 2529.
42. K. H. Song, C. B. Highley, A. Rouff and J. A. J. A. F. M. Burdick, 2018, **28**, 1801331.
43. T. J. Hinton, Q. Jallerat, R. N. Palchesko, J. H. Park, M. S. Grodzicki, H.-J. Shue, M. H. Ramadan, A. R. Hudson and A. W. J. S. a. Feinberg, 2015, **1**, e1500758.
44. O. Jeon, Y. B. Lee, H. Jeong, S. J. Lee, D. Wells and E. J. M. h. Alsberg, 2019, **6**, 1625-1631.
45. N. Noor, A. Shapira, R. Edri, I. Gal, L. Wertheim and T. Dvir, *Adv Sci (Weinh)*, 2019, **6**, 1900344.
46. A. C. Daly, G. M. Cunniffe, B. N. Sathy, O. Jeon, E. Alsberg and D. J. J. A. h. m. Kelly, 2016, **5**, 2353-2362.
47. M. A. Heinrich, R. Bansal, T. Lammers, Y. S. Zhang, R. Michel Schiffelers and J. Prakash, *Adv. Mater.*, 2019, **31**, e1806590.
48. A. Shapira and T. Dvir, *Adv Sci (Weinh)*, 2021, **8**, 2003751.
49. T. J. Hinton, A. Lee and A. W. Feinberg, *Current Opinion in Biomedical Engineering*, 2017, **1**, 31-37.
50. A. Maton, *Human biology and health*, Prentice Hall, 1997.
51. J. M. Lee, W. L. Ng and W. Y. Yeong, *Applied Physics Reviews*, 2019, **6**.
52. H. Freundlich and L. J. K.-Z. Bircumshaw, 1926, **40**, 19-22.
53. J. Mewis, N. J. J. A. i. c. Wagner and i. science, 2009, **147**, 214-227.
54. A. K. Grosskopf, R. L. Truby, H. Kim, A. Perazzo, J. A. Lewis and H. A. Stone, *ACS Appl Mater Interfaces*, 2018, **10**, 23353-23361.
55. M. Wehner, R. L. Truby, D. J. Fitzgerald, B. Mosadegh, G. M. Whitesides, J. A. Lewis and R. J. Wood, *Nature*, 2016, **536**, 451-455.
56. J. T. Muth, D. M. Vogt, R. L. Truby, Y. Menguc, D. B. Kolesky, R. J. Wood and J. A. Lewis, *Adv. Mater.*, 2014, **26**, 6307-6312.
57. J. Mewis and N. J. Wagner, *Adv. Colloid Interface Sci.*, 2009, **147-148**, 214-227.
58. C. B. Highley, C. B. Rodell and J. A. Burdick, *Adv. Mater.*, 2015, **27**, 5075-5079.
59. K. H. Song, C. B. Highley, A. Rouff and J. A. Burdick, *Adv. Funct. Mater.*, 2018, **28**.
60. L. Shi, H. Carstensen, K. Hölzl, M. Lunzer, H. Li, J. Hilborn, A. Ovsianikov and D. A. Ossipov, *Chemistry of Materials*, 2017, **29**, 5816-5823.
61. C. S. O'Bryan, T. Bhattacharjee, S. R. Niemi, S. Balachandar, N. Baldwin, S. T. Ellison, C. R. Taylor, W. G. Sawyer and T. E. Angelini, *MRS Bull.*, 2017, **42**, 571-577.
62. B. Gueslin, L. Talini, B. Herzhaft, Y. Peysson and C. Allain, *Phys. Fluids*, 2006, **18**.
63. A. M. V. Putz, T. I. Burghelena, I. A. Frigaard and D. M. Martinez, *Phys. Fluids*, 2008, **20**.
64. T. Uchida and H. Onoe, *Micromachines (Basel)*, 2019, **10**.
65. R. L. Mauck, C. C. Wang, E. S. Oswald, G. A. Ateshian and C. T. Hung, *Osteoarthritis Cartilage*, 2003, **11**, 879-890.
66. R. Sharma, R. Kirsch, K. P. Valente, M. R. Perez and S. M. Willerth, *Processes*, 2021, **9**.
67. T. Bhattacharjee, S. M. Zehnder, K. G. Rowe, S. Jain, R. M. Nixon, W. G. Sawyer and T. E. Angelini, *Sci Adv*, 2015, **1**, e1500655.
68. T. J. Hinton, Q. Jallerat, R. N. Palchesko, J. H. Park, M. S. Grodzicki, H. J. Shue, M. H. Ramadan, A. R. Hudson and A. W. Feinberg, *Sci Adv*, 2015, **1**, e1500758.
69. A. Lee, A. R. Hudson, D. J. Shiwarski, J. W. Tashman, T. J. Hinton, S. Yerneni, J. M. Bliley, P. G. Campbell and A. W. Feinberg, *Science*, 2019, **365**, 482-487.
70. O. Jeon, Y. B. Lee, H. Jeong, S. J. Lee, D. Wells and E. Alsberg, *Mater Horiz*, 2019, **6**, 1625-1631.
71. E. C. Cho, J. W. Kim, A. Fernandez-Nieves and D. A. Weitz, *Nano Lett.*, 2008, **8**, 168-172.
72. J. D. Debord, S. Eustis, S. Byul Debord, M. T. Lofye and L. A. Lyon, *Advanced Materials*, 2002, **14**, 658-662.
73. A. M. Compaan, K. Song, W. Chai and Y. Huang, *ACS Appl Mater Interfaces*, 2020, **12**, 7855-7868.
74. A. Shapira, N. Noor, H. Oved and T. Dvir, *Biomed Mater*, 2020, **15**, 045018.
75. S. R. Moxon, M. E. Cooke, S. C. Cox, M. Snow, L. Jeys, S. W. Jones, A. M. Smith and L. M. Grover, *Adv. Mater.*, 2017, **29**.
76. D. Bi, J. Zhang, B. Chakraborty and R. P. Behringer, *Nature*, 2011, **480**, 355-358.
77. A. J. Liu and S. R. Nagel, *Nature*, 1998, **396**, 21-22.
78. C. Pellet and M. Cloitre, *Soft Matter*, 2016, **12**, 3710-3720.
79. P. Coussot, L. Tocquer, C. Lanos and G. Ovarlez, *Journal of Non-Newtonian Fluid Mechanics*, 2009, **158**, 85-90.
80. H. Mehrabian and J. J. J. o. F. M. Feng, 2013, **717**, 281.
81. E. Pairam, H. Le and A. Fernandez-Nieves, *Phys Rev E Stat Nonlin Soft Matter Phys*, 2014, **90**, 021002.
82. C. S. O'Bryan, T. Bhattacharjee, S. Hart, C. P. Kabb, K. D. Schulze, I. Chilakala, B. S. Sumerlin, W. G. Sawyer and T. E. Angelini, *Sci Adv*, 2017, **3**, e1602800.
83. C. S. O'Bryan, A. Brady-Mine, C. J. Tessmann, A. M. Spatz and T. E. Angelini, *Soft Matter*, 2021, **17**, 3886-3894.
84. C. S. O'Bryan, T. Bhattacharjee, S. L. Marshall, W. Gregory Sawyer and T. E. Angelini, *Bioprinting*, 2018, **11**.
85. K. Holzl, S. Lin, L. Tytgat, S. Van Vlierberghe, L. Gu and A. Ovsianikov, *Biofabrication*, 2016, **8**, 032002.
86. A. Blaeser, D. F. Duarte Campos, U. Puster, W. Richtering, M. M. Stevens and H. Fischer, *Adv Healthc Mater*, 2016, **5**, 326-333.
87. M. E. Cooke and D. H. Rosenzweig, *APL Bioeng*, 2021, **5**, 011502.
88. S. Chen, T. S. Jang, H. M. Pan, H. D. Jung, M. W. Sia, S. Xie, Y. Hang, S. K. M. Chong, D. Wang and J. Song, *Int J Bioprint*, 2020, **6**, 258.
89. B. Webb and B. J. Doyle, *Bioprinting*, 2017, **8**, 8-12.
90. J. Lewicki, J. Bergman, C. Kerins and O. Hermanson, *Bioprinting*, 2019, **16**.
91. O. Jeon, Y. Bin Lee, T. J. Hinton, A. W. Feinberg and E. Alsberg, *Mater Today Chem*, 2019, **12**, 61-70.

92. D. N. Heo, M. A. Alioglu, Y. Wu, V. Ozbolat, B. Ayan, M. Dey, Y. Kang and I. T. Ozbolat, *ACS Appl Mater Interfaces*, 2020, **12**, 20295-20306.
93. I. T. Ozbolat, *Trends Biotechnol.*, 2015, **33**, 395-400.
94. M. Hospodiuk, M. Dey, D. Sosnoski and I. T. Ozbolat, *Biotechnol. Adv.*, 2017, **35**, 217-239.
95. M. Dey and I. T. Ozbolat, *Sci Rep*, 2020, **10**, 14023.
96. T. Billiet, E. Gevaert, T. De Schryver, M. Cornelissen and P. Dubruel, *Biomaterials*, 2014, **35**, 49-62.
97. K. Y. Lee and D. J. Mooney, *Prog. Polym. Sci.*, 2012, **37**, 106-126.
98. Y. B. Lee, O. Jeon, S. J. Lee, A. Ding, D. Wells and E. Alsborg, *Adv. Funct. Mater.*, 2021, **31**.
99. V. Mironov, R. P. Visconti, V. Kasyanov, G. Forgacs, C. J. Drake and R. R. Markwald, *Biomaterials*, 2009, **30**, 2164-2174.
100. Y. Yu, K. K. Moncal, J. Li, W. Peng, I. Rivero, J. A. Martin and I. T. Ozbolat, *Sci Rep*, 2016, **6**, 28714.
101. Y. Wu, M. Hospodiuk, W. Peng, H. Gudapati, T. Neuberger, S. Koduru, D. J. Ravnica and I. T. Ozbolat, *Biofabrication*, 2018, **11**, 015009.
102. A. N. Leberfinger, D. J. Ravnica, A. Dhawan and I. T. Ozbolat, *Stem Cells Transl Med*, 2017, **6**, 1940-1948.
103. E. A. Bulanova, E. V. Koudan, J. Degosserie, C. Heymans, F. D. Pereira, V. A. Parfenov, Y. Sun, Q. Wang, S. A. Akhmedova, I. K. Sviridova, N. S. Sergeeva, G. A. Frank, Y. D. Khesuani, C. E. Pierreux and V. A. Mironov, *Biofabrication*, 2017, **9**, 034105.
104. B. Ayan, D. N. Heo, Z. Zhang, M. Dey, A. Povilianskas, C. Drapaca and I. T. Ozbolat, *Sci Adv*, 2020, **6**, eaaw5111.
105. B. Ayan, N. Celik, Z. Zhang, K. Zhou, M. H. Kim, D. Banerjee, Y. Wu, F. Costanzo and I. T. Ozbolat, *Commun Phys*, 2020, **3**.
106. J. S. Miller, *PLoS Biol.*, 2014, **12**, e1001882.
107. E. Mirdamadi, J. W. Tashman, D. J. Shiwerski, R. N. Palchesko and A. W. Feinberg, *ACS Biomaterials Science & Engineering*, 2020, **6**, 6453-6459.
108. L. Ning and X. Chen, *Biotechnol J*, 2017, **12**.
109. M. A. Skylar-Scott, J. Mueller, C. W. Visser and J. A. Lewis, *Nature*, 2019, **575**, 330-335.
110. J. Y. Park, J. C. Choi, J. H. Shim, J. S. Lee, H. Park, S. W. Kim, J. Doh and D. W. Cho, *Biofabrication*, 2014, **6**, 035004.
111. H. W. Kang, S. J. Lee, I. K. Ko, C. Kengla, J. J. Yoo and A. Atala, *Nat. Biotechnol.*, 2016, **34**, 312-319.
112. Y. Zhao, R. Yao, L. Ouyang, H. Ding, T. Zhang, K. Zhang, S. Cheng and W. Sun, *Biofabrication*, 2014, **6**, 035001.
113. B. Duan, L. A. Hockaday, K. H. Kang and J. T. Butcher, *J. Biomed. Mater. Res. A*, 2013, **101**, 1255-1264.
114. A. M. Compaan, K. Song and Y. Huang, *ACS Appl Mater Interfaces*, 2019, **11**, 5714-5726.
115. K. Hajash, B. Sparrman, C. Guberan, J. Laucks and S. Tibbits, *3D Printing and Additive Manufacturing*, 2017, **4**, 123-132.
116. A. Ovsianikov, J. Yoo and V. Mironov, *3D printing and biofabrication*, Springer, 2018.
117. W. Y. Yeong and C. K. Chua, *Bioprinting: principles and applications*, World Scientific Publishing Co Inc, 2014.
118. D. J. Shiwerski, J. W. Tashman, A. F. Eaton, G. Apodaca and A. W. Feinberg, *HardwareX*, 2020, **7**.
119. T. J. Hinton, A. Hudson, K. Pusch, A. Lee and A. W. Feinberg, *ACS Biomater Sci Eng*, 2016, **2**, 1781-1786.
120. K. Zhu, S. R. Shin, T. van Kempen, Y. C. Li, V. Ponraj, A. Nasajpour, S. Mandla, N. Hu, X. Liu, J. Leijten, Y. D. Lin, M. A. Hussain, Y. S. Zhang, A. Tamayol and A. Khademhosseini, *Adv. Funct. Mater.*, 2017, **27**.
121. Y. Jin, A. Compaan, T. Bhattacharjee and Y. Huang, *Biofabrication*, 2016, **8**, 025016.